

SUPPORTING INFORMATION

Chiral Smectic Structure Assembled by Nanosheets and Nanorods

by H. Pan and S. Zhu *et al.*

1. Experimental Method

1.1 Synthesis and fabrication

1.1.1 Preparation of graphene oxide

Step 1. Graphene oxide (GO) was prepared by the modified Hummers method.¹⁻³ In an ice-water bath, 10 g flake graphite (325 mash, Nanjing XFNANO Materials Tech Inc.) was added into 230 mL concentrated H₂SO₄ in which dissolved 10 g KNO₃. After stirring for 0.5 h at 10~15 °C, the temperature was increased to 40 °C and kept stirring for 3.5 h. Then, the mixture was diluted with deionized (DI) water. After centrifuging, the precipitate was dried to get the preprocessed graphite. All other chemical agents (analytic grade) used in this study were supplied by Sinopharm Inc.

Step 2. In an ice-water bath, 30 g KMnO₄ was slowly added into 230 mL concentrated H₂SO₄. Then, the preprocessed graphite obtained in Step 1 was added. After stirring at 40 °C for 2 h, the mixture was diluted with 250 mL DI water. Subsequently, dropwise adding of H₂O₂ resulted in reduction of the residual KMnO₄. The obtained graphene oxide was washed with 5% HCl and then with DI water for several times. After dialyzing with cellulose membrane for 7 days, the pure graphene oxide with low concentration was obtained. The concentration of GO was measured by weight method.

1.1.2 Preparation of CNC

CNCs were prepared by acid hydrolysis method from cotton.⁴⁻⁶ Typically, 10 g cotton was added into 5% NaOH solution (aq.) to degrease for 2 h. The degreased cotton was hydrolyzed in 50% H₂SO₄ at 65 °C for 1.5 h. The hydrolysate was washed for several times with DI water. Then, dialyzing with cellulose membrane (molecule weight cut-off 14,000 ± 2,000, Shanghai Yuanju Company) for 5 days and the pure CNCs with low concentration were obtained.

1.1.3 Preparation of CNC/GO composite colloids, films and fibers

We developed a “single-particle-level mixing” method to prepare highly dispersed colloid with extremely high concentration. In order to prevent aggregation of nanoparticles, CNC and GO colloids were mixed at very low concentration (<0.1 wt%). Cross-linked polyacrylate hydrogel (Aladdin Inc.) was employed to concentrate the blended suspension under slightly shaking. When the concentration of the blended colloid was up to a certain value (3~5 wt%), the hydrogel was removed. The obtained colloid was further concentrated by centrifugation with a rotation speed of 10,000 r min⁻¹. A highly concentrated composite colloid was thus obtained. As compared with directly dissolving solid powder in a liquid by sonication, this method preparing highly concentrated colloid starts from very low concentration, ensuring the compositing at single-particle level. This method is also time-saving and straightforward than traditional means, e.g. heating.⁷

The CNC/GO films were prepared at low concentration (~2 wt%) by spin-coating the colloids on PET substrate and then dried in an oven at 60 °C. CNC/GO fibers were fabricated by the typical wet-spinning method.⁸ A spinneret with 150 μm inner diameter was used. The acetone was used as coagulating bath.

1.2 Characterization

1.2.1 Structure characterization

Zeta potential of diluted colloids (0.01 wt%) was measured using a Zetasizer Nano ZS (Mastersizer 2000E, Malvern) without adjusting ionic strength. Polarizing microscopy (POM, VHM-3201 OLYMPUS) was used to study the structure of CNC/GO colloids. Typically, the colloids were fixed between two large pieces of glass, which were subject to homogenous planar boundary condition. The thickness of the films and the diameter of the fibers were measured by a thickness tester (AICE Inc.). The size and morphologies of GO, CNC and CNC/GO were observed by atomic force microscopy (AFM, Nanonavi E-Sweep SII). The diluted suspensions were dropped on mica sheet for observation. A diamond tip and a smart mode were employed for the test. Scanning electron microscopy (SEM, JSM-6360LV JEOL) was used to observe the morphology of films and fibers. The samples for SEM test were firstly treated by gold-spraying for 40 s. The accelerating voltage was 5 kV. The chirality of the colloids was studied by a Circular Dichroism spectrometer (CD, J-815 JASCO). A Dispersive Raman Microscope (Senterra R200-L Bruker Optics) with 532 nm laser was used to record the Raman spectra. FTIR spectra were collected on a Nicolet 6700 spectrometer (Thermo Fisher) with a Ge crystal ATR accessory. Synchrotron radiation small-angle X-ray scattering (SAXS) was used to reveal the structures of the CNC/GO colloids. Generally, the samples were filled in a liquid cell which was covered by polyimide film. The SAXS patterns were obtained on the BL16B1 beamline at the Shanghai Synchrotron Radiation Facility (SSRF, photon flux $\approx 1 \times 10^{11}$, beam size $\leq 0.4 \times 0.8$ mm). The experiment was performed with a wavelength λ of 0.124 nm and a sample-to-detector distance of 2,500 mm. The exposure time is 20 s. The solvent water was used for background collection. The chicken tendon was used for calibration. The WAXD patterns were collected on the BL16B1 beamline at a sample-to-detector distance of 119 mm. The exposure time is 1 s and air was chosen for background. The CeO₂ (PDF NO. 34-0394) powder was used for calibration. FIT2D software (V12.077) was used to process the SAXS and WAXD patterns.

1.2.2 Phase diagram plotting

A series of CNC/GO colloids with varying χ_{CNC} from 0 to 1 were prepared. The χ_{CNC} was set to 0, 10%, 20%, 30%, 40%, 50%, 60%, 70%, 80%, 90% and 100%. Each sample was first concentrated to high concentration. The fluidity of the colloids in this work was used to estimate the transformation of colloids to gel or solid. Thus, the line E-F in Figure 2 was plotted. By using a polarized optical microscopy, the colloids were observed with decreasing concentration by quantitative dilution. Samples were detected by small angle X-ray scattering to confirm the laminar structure. The phases were evaluated according to the SAXS results and POM textures through comparison with texture library.

2. Supplementary Information and Discussion

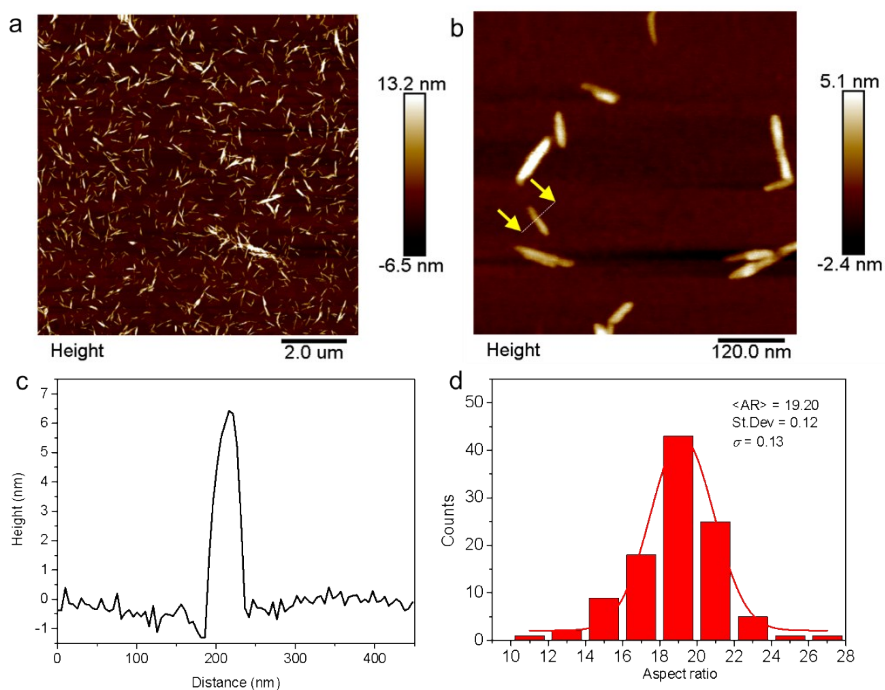


Figure S1. (a,b) AFM image of CNCs at different magnification. (c) Height profiles corresponding to the lines in (b). (d) Aspect ratio distribution of CNCs.

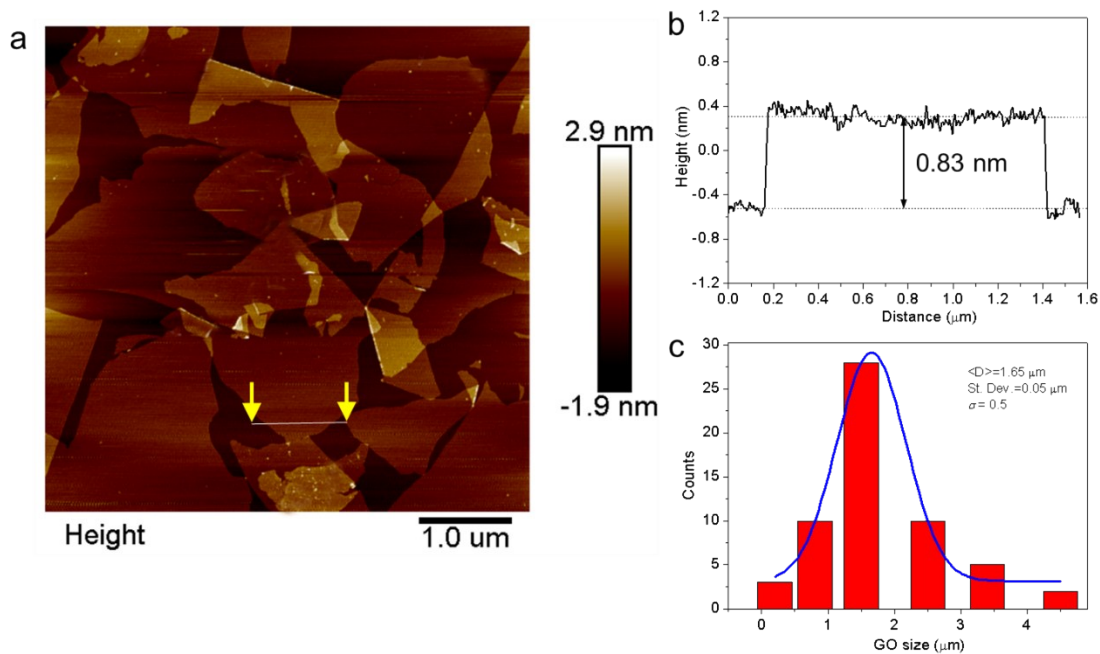


Figure S2. (a) AFM image of GO. (b) Height profile corresponding to the line in (a). (c) Size distribution of GO.

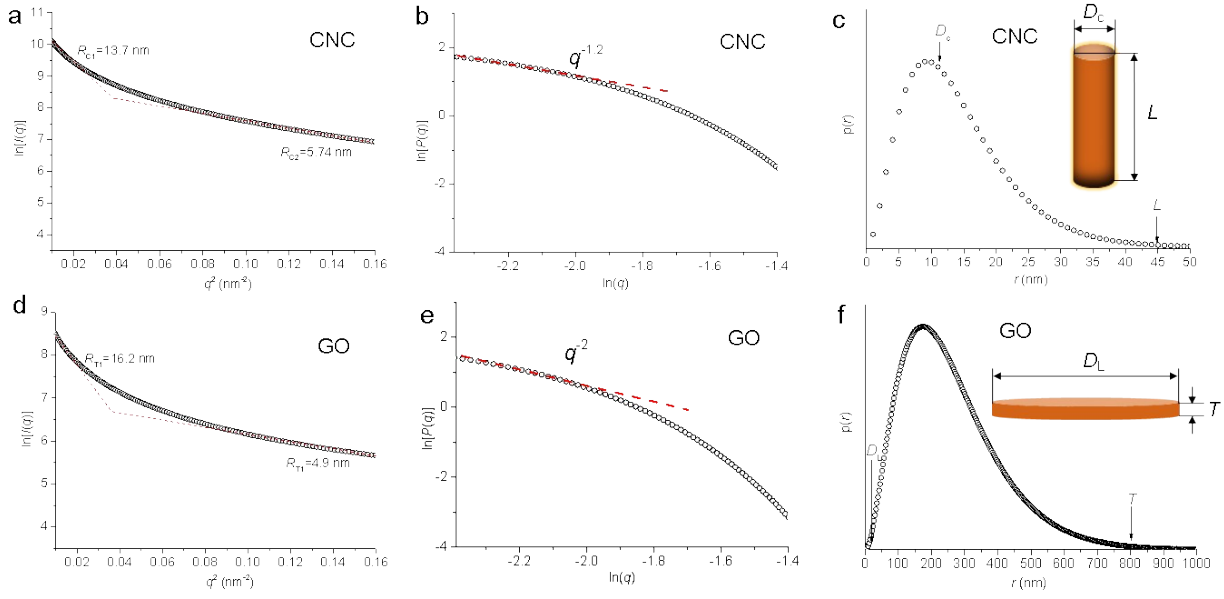


Figure S3. Shape and size of CNCs and GO extracted from small angle regions (Guinier regions) of SAXS data. (a,d) $\ln[I(q)]-q^2$ curves (Guinier diagram), (b,e) $\ln[P(q)]-\ln q$ curves (particle form factor diagram) and (c,f) Pair-distance distribution function of CNCs and GO, respectively.

Figure S3 shows the shape and size of CNCs and GO obtained from the SAXS data. For extremely dilute isotropic solution, the radius of gyration (R_g , here R_C for CNCs and R_T for GO) can be obtained from the Guinier profile:⁹

$$I(q) = a_0 \exp\left(-\frac{R_g^2}{3} q^2\right) \quad (\text{S1})$$

where q is scattering vector, $I(q)$ is the scattering intensity, and a_0 is a constant. Take the logarithm of Equation S1:

$$\ln[I(q)] = \ln a_0 - \frac{R_g^2}{3} q^2 \quad (\text{S2}).$$

Hence, R_g can be obtained from the slope of $\ln[I(q)]-q^2$ curve in a small q region, shown in Figure S3a,d. In this work, the R_C for CNCs is 13.7 nm and R_T for GO is 16.2 nm. The R_g in a larger q region (R_{C2} , R_{T2}) is caused by the partial aggregation of nanoparticles. The form factor $P(q)$ can be approximated by a Gaussian function as follows:¹⁰

$$P(q) \approx a_0 \exp\left(-\frac{R_g^2}{3} q^2\right) \quad (\text{S3})$$

where a_0 is given from the intercept of S2. For cylindrical particles, $P(q)$ is expressed as:

$$P(q) = \frac{a_0}{q} \exp\left(-\frac{R_C^2}{2} q^2\right) \quad (\text{S4})$$

while for lamellar particles, $P(q)$ is expressed as:

$$P(q) = \frac{a_0}{q^2} \exp(-R_r^2 q^2) \quad (\text{S5}).$$

According to the power law of $\ln[P(q)] - \ln q$, we can estimate the shape of the particles, 0, -1 or -2 which respectively indicate globular, cylindrical or lamellar shape. As shown in Figure S3b and e, it can be seen that the powers of CNCs and GO are -1.2 and -2, indicating the cylindrical and lamellar shape of CNCs and GO, respectively.

In order to obtain the size information, we further investigated the pair-distance distribution functions $p(r)$ of CNCs and GO. According to the Debye-Bueche theory:

$$I(q) = C \int_0^\infty r^2 \gamma(r) \frac{\sin qr}{qr} dr \quad (\text{S6})$$

where $\gamma(r)$ is correlation function and C is constant. $r^2 \gamma(r)$ is defined as the pair-distance distribution function:

$$p(r) = r^2 \gamma(r) \quad (\text{S7})$$

For cylindrical shape, $\gamma(r)$ can be approximated by an exponential function:

$$\gamma(r) = e^{-r/a} \quad (\text{S8})$$

where a is constant. By using Equation S8 for Equation S6, we have:

$$I(q) = C \int_0^\infty r^2 e^{-r/a} \frac{\sin qr}{qr} dr = K \frac{a^3}{(1+a^2 q^2)^2} \quad (\text{S9})$$

where K is constant. Equation S9 can be transformed into:

$$[I(q)]^{-1/2} = K^{-1/2} \frac{1+a^2 q^2}{a^{3/2}} \quad (\text{S10}).$$

Plotting $[I(q)]^{-1/2}$ against q^2 , a can be obtained from the slope and intercept:

$$a = \left(\frac{\text{Slope}}{\text{Intercept}} \right)^{1/2} \quad (\text{S11}).$$

Hence, we obtain $p(r)$ of CNCs shown in Figure S3c. The particle size can be estimated from the feature-points in $p(r)$ curve. It shows a diameter of 10–15 nm and length >45 nm for CNCs.

For lamellar shape, $\gamma(r)$ can be approximated by a Gaussian function:

$$\gamma(r) = e^{-r^2/a^2} \quad (\text{S12})$$

where a is constant. By using S12 for S6, we have:

$$I(q) = C_1 a^3 e^{-q^2 a^2 / 4} \quad (\text{S13})$$

where C_1 is constant. Take the logarithm of Equation S13:

$$\ln[I(q)] = C_2 - \frac{a^2}{4}q^2 \quad (\text{S14})$$

where C_2 is constant. Therefore, a can be obtained from the slope of the $\ln[I(q)]-q^2$ curve. Substitute a into S12 and further S12 into S7, we have the $p(r)$ of GO shown in Figure S3f. It shows a thickness of ~ 10 nm and diameter >800 nm for GO. However, we can see the difference between the results from microscopy techniques and SAXS. It is a well-known challenge to obtain accurate size information from X-ray scattering for polydispersed systems. The inaccuracy would be caused by the approximation and error accumulation throughout the calculation.

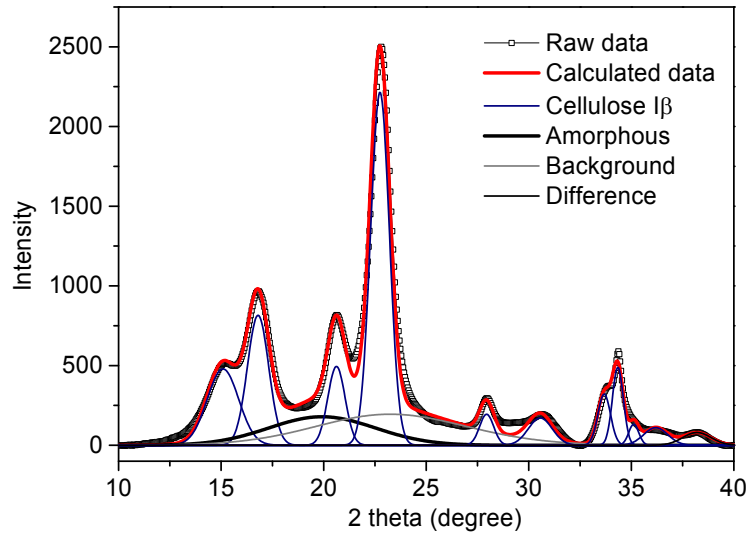


Figure S4. Rietveld fitted XRD pattern of CNC.

According to the references,¹¹⁻¹⁴ the crystalline type of CNC in this work is assigned to monoclinic P21 cellulose I β with cell parameters ($a = 0.7784$ nm, $b = 0.8021$ nm, $c = 1.0380$ nm, $\alpha = \beta = 90^\circ$, $\gamma = 96.5^\circ$). The characteristic peaks centered at $2\theta = 15.8^\circ$, 16.8° , 20.6° , 22.8° and 34.6° are corresponding to (1 -1 0), (1 1 0), (0 1 2), (2 0 0), and (0 0 4), respectively. Rietveld method was conducted to obtain crystallinity (X_c).¹⁵ Gaussian and Voigt shapes were used for crystal peaks and amorphous peak respectively. A three-parameter second order polynomial function was used for the background. X_c is calculated by the equation:¹⁶

$$X_c = 1 - \frac{A_a}{A_s - A_b} = 1 - \frac{\int_{2\theta_1}^{2\theta_2} I_a d(2\theta)}{\int_{2\theta_1}^{2\theta_2} (I_s - I_b) d(2\theta)} \quad (\text{S15})$$

where A_a , A_b and A_s are the area values of the amorphous, the background and the whole pattern, respectively; I_a , I_b and I_s respectively refer to their intensity values. The crystallinity of CNC is about 78% in this work.

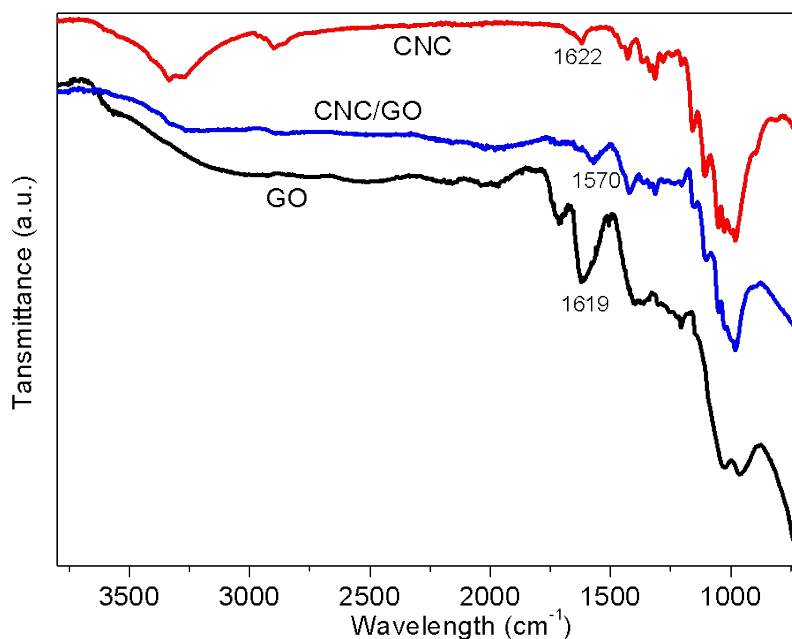


Figure S5. FTIR spectra of GO, CNC and CNC/GO.

Figure S5 shows the FTIR spectra of GO, CNC and CNC/GO composite. The broad band at around 3000-3700 cm^{-1} can be assigned to the O-H stretching vibration. The peaks at 3334 cm^{-1} and 3269 cm^{-1} can be attributed to OH group of free water or the pyranose rings of CNC. In terms of CNC, the peaks at around 1050 cm^{-1} are corresponding to the C-O stretching vibrations (alkoxy groups). The absorbance peak at 1004 cm^{-1} is ascribed to the C-O stretching in CNC introduced during the sulfuric acid hydrolysis.^{17, 18} As for GO, the absorbent peaks of oxygen-containing functional groups appear at 1027, 1210, and 1381 cm^{-1} , caused by the C-O vibration of alkoxide, epoxy/ether, and hydroxyl groups, respectively.¹⁹ It should be mentioning that the band of intramolecular hydrogen bond appears at 1622 and 1619 cm^{-1} in CNC and GO, respectively.²⁰ Interestingly, the band of intramolecular hydrogen bond in CNC/GO shifts about 50 cm^{-1} to 1570 cm^{-1} . This shift may be attributed to the increased hydrogen bonds formed between CNC and GO in the composite. The change of chemical environment can induce the shift of absorbance peaks, as reported by many others.^{19, 21} Therefore, the interaction between CNC and GO in self-assembled CNC/GO system is evidenced by the analysis of FTIR results.

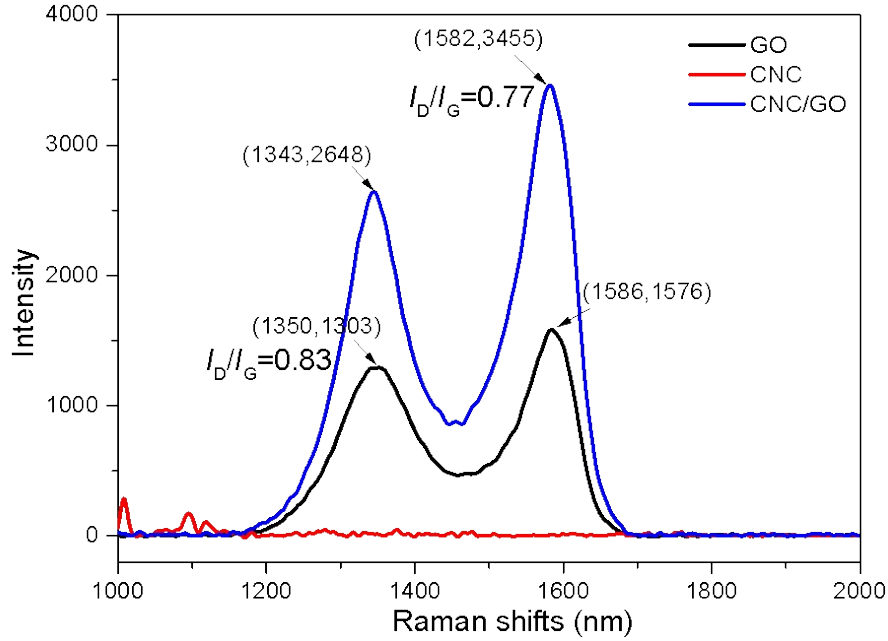


Figure S6. Raman spectra of GO, CNC and CNC/GO.

In Raman spectrum of GO, the D band at 1350 cm⁻¹ is assigned to the breathing mode of κ -point phonons with A_{1g} symmetry, while the G band 1586 cm⁻¹ is attributed to the tangential stretching mode of the E_{2g} phonon of the carbon sp² atoms.²² The D peak is from the structural imperfections, e.g. hydroxyl and epoxide groups on the carbon basal plane.²³ As for the sample CNC/GO, a slight shift in wavenumber is observed for both D and G bands as compared with GO. This would be explained by the interaction formed between CNC and GO, as described in other GO-based composites reported.²⁴ Additionally, the intensity ratio of D and G bands (I_D/I_G) was observed decrease for CNC/GO (0.77) in comparison with GO (0.83). This decrease may be related to an increase in the order degree of CNC/GO matrix,²⁰ in part due to the interaction (hydrogen bonds) caused changes in chemical environment of defect carbon sp³ atoms.

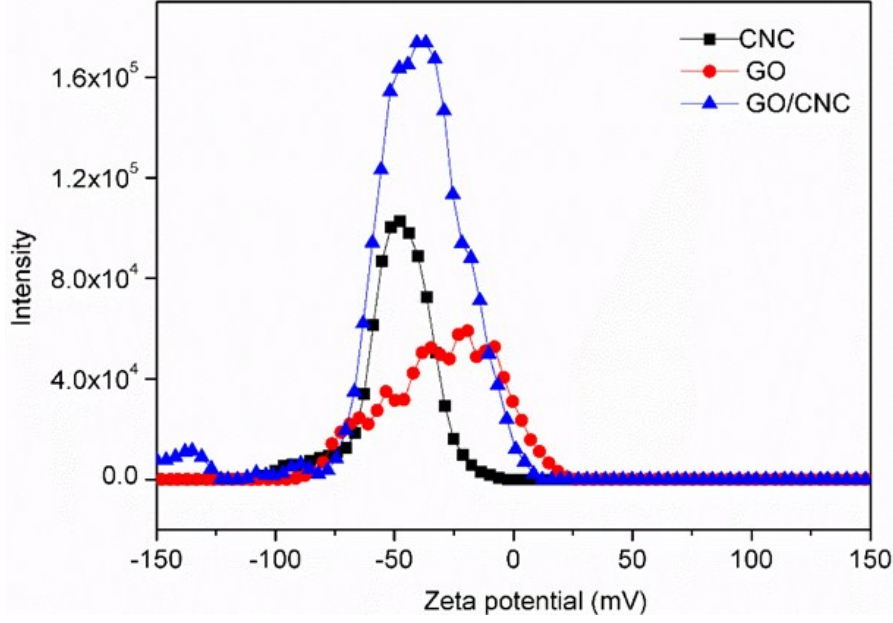


Figure S7. Zeta potentials of (a) CNC, (b) GO and (c) CNC/GO composite (weight ratio of CNC/GO is 1). CNC suspension has a Zeta potential of $-(50 \pm 3)$ mV while that of GO is $-(37 \pm 6)$ mV. The CNC/GO composite shows a $-(45 \pm 5)$ mV Zeta potential.

We used titration to determine the surface charge density S of CNCs and GO suspensions. CNCs and GO were approximated to cylinder and plate, of which geometric dimensions were obtained from AFM data. The mass density of CNC and GO are 1.6 and 1.06 g cm^{-3} , respectively. The number of particles is determined by the equation:

$$N_x = \frac{m_x c_x}{\rho_x V_x} \quad (\text{S16})$$

where N_x is the number of particles, m_x the mass of suspension, c_x the mass concentration of suspension, ρ_x the mass density of nanoparticles and V_x the volume of a single particle. Hence, the surface charge density can be calculated by:

$$\delta = \frac{n(\text{OH}^-) V(\text{OH}^-) N_A}{N_x S_x} \quad (\text{S17})$$

where $n(\text{OH}^-)$ is the molar concentration of NaOH, $V(\text{OH}^-)$ is the volume of consumed NaOH, N_A is Avogadro constant and S_x is the surface area of single particle. The surface charge of CNCs suspension is 0.15 e nm^2 , which is similar to that estimated by Dong *et al.*²⁵ The surface charge of GO suspension is 66.5 e nm^2 in this work.

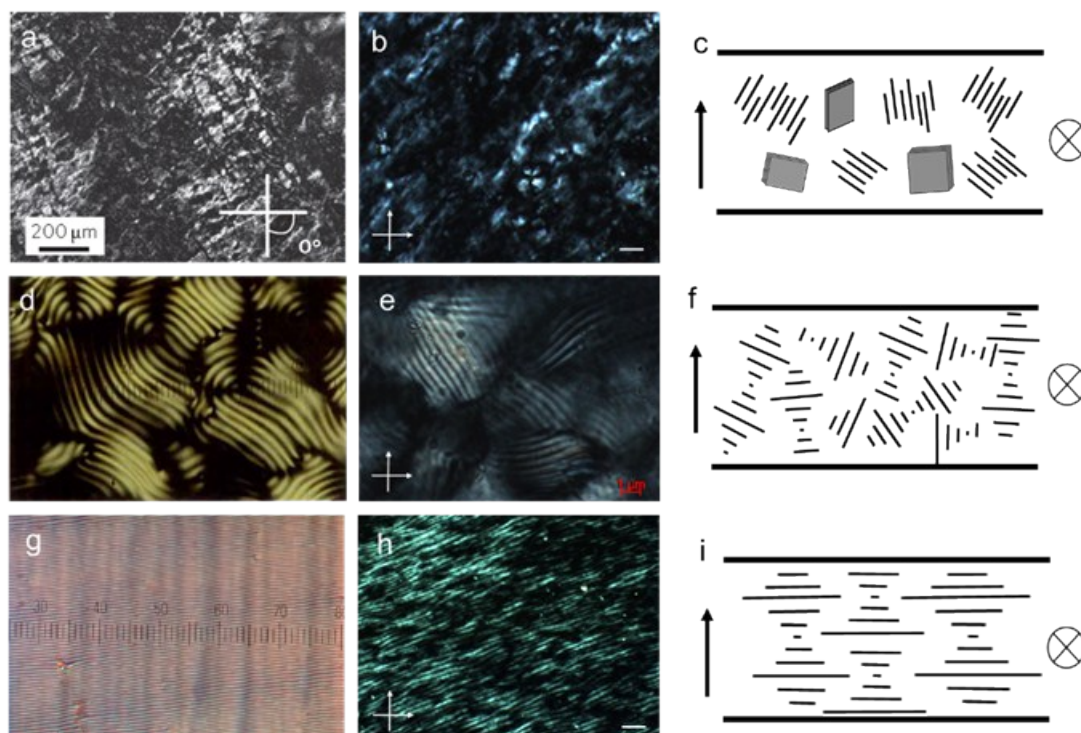


Figure S8. Texture comparison and schematic illustration of chiral structures.

Figure S8a is POM image of GO colloid with a concentration of ~ 2 wt%. Schlieren texture is assigned to discotic nematic structure. Behabtu *et al.*, *Nat. Nanotech.*, 2010, 5, 406. Figure S8b is POM image of GO colloid in this work. It shows schlieren texture very similar to (a). Figure S8c schematically illustrates the discotic nematic arrangements in thin cells for POM observation. The black arrow represents the incident polarized light and “ \otimes ” indicates the observation direction. Figure S8d is characteristic fingerprint texture of a chiral nematic observed in the polarizing microscope. D. Demus, *Handbook of Liquid Crystals*, 1998, pp457. Copyright WILEY-VCH Verlag GmbH. The original figure was reported by P. Haurand, Dissertation, TU Clausthal, Clausthal-Zellerfeld, Germany 1990. Figure S8e is the fingerprint texture observed in CNC colloid in this work. It is highly similar to (d). Figure S8f is schematic illustration of chiral nematic arrangements in thin cell for POM observation. Figure S8g is the banded texture of a chiral smectic C (SmC*), **Plate 77** in *Textures of Liquid Crystals*, Ingo Dierking, Copyright WILEY-VCH Verlag GmbH & Co. KGaA, Weinheim 2003, pp193. The original figure was reported by I. Dierking *et al.*, *Liq. Cryst.*, 1993, 13, 45. <http://www.tandf.co.uk/Journals>. Figure S8h is the texture of CNC/GO colloid in this work. It shows apparent banded texture similar to that in (g). Figure S8i schematically shows the chiral smectic arrangements in thin cell for POM observation.

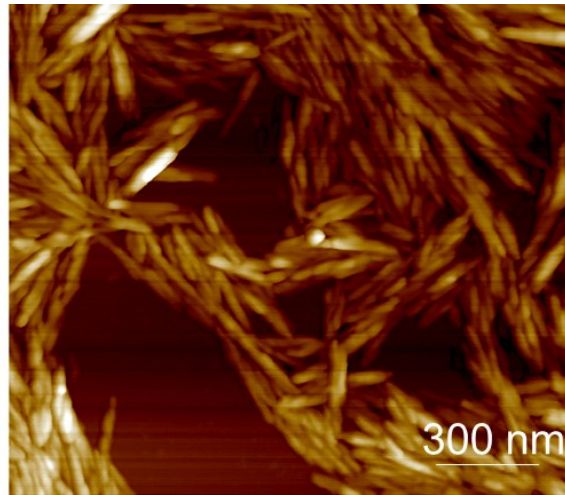


Figure S9. AFM images of CNCs self-assembled on GO substrate.

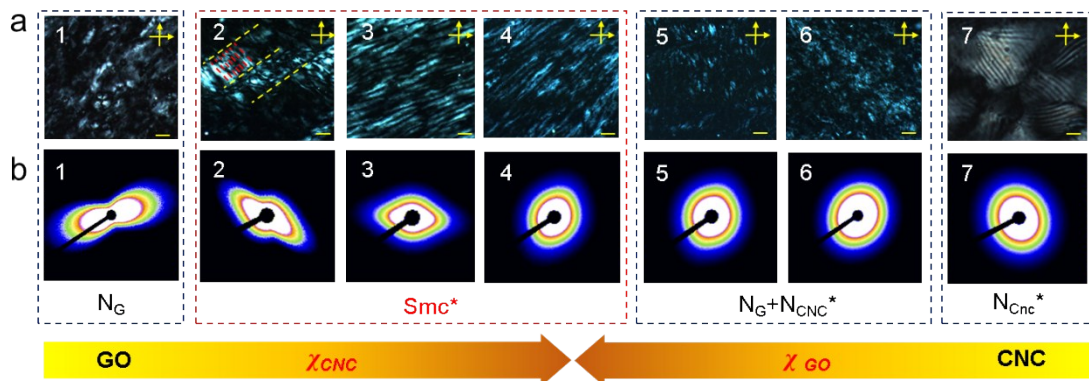


Figure S10. (a) POM of GO, CNC and CNC/GO colloids with different weight fractions. The numbers 1-7 represent GO, CNC/GO (2:8 wt), CNC/GO (4:6 wt), CNC/GO (5:5 wt), CNC/GO (6:4 wt), CNC/GO (8:2 wt) and CNC, respectively. The concentrations of the suspensions range from 4% to 5%. Scale bar 10 μm . (b) Two-dimensional SAXS patterns of the samples shown in (a).

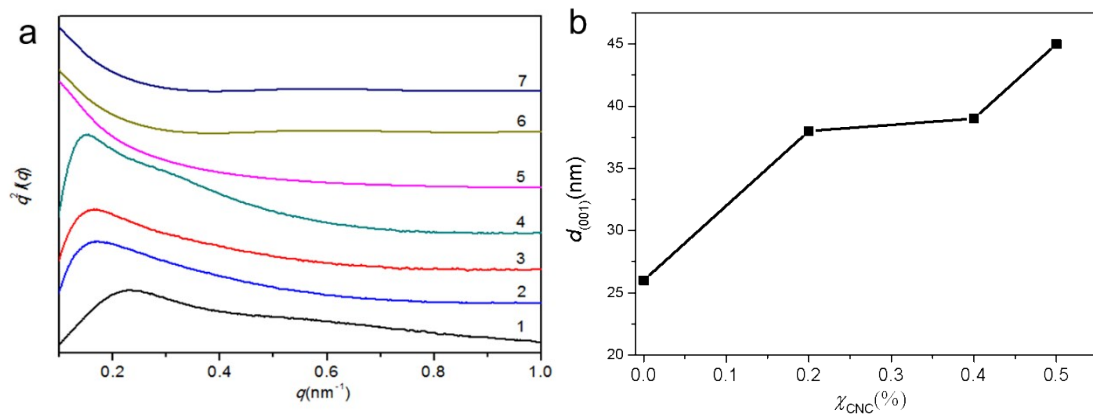


Figure S11. (a) One-dimensional SAXS patterns of the samples shown in Figure S10b. (b) The interlayer spacing $d_{(001)}$ plotted against the CNC content.

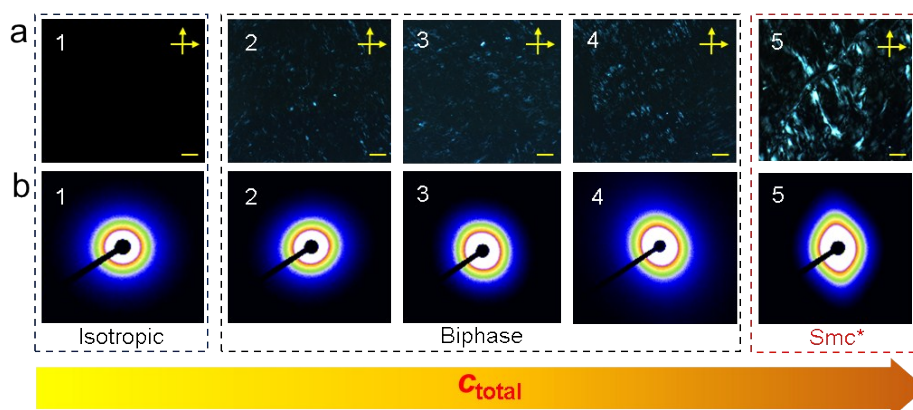


Figure S12. (a) POM of CNC/GO colloids with different total concentrations (c_{total}). The numbers 1-5 represent c_{total} values of 0.2 wt%, 0.5 wt%, 0.9 wt%, 1.2 wt%, and 1.5 wt%, respectively. The weight fraction is 3:7 (CNC/GO wt). Scale bar 10 μm . (b) Two-dimensional SAXS patterns of the samples shown in (a).

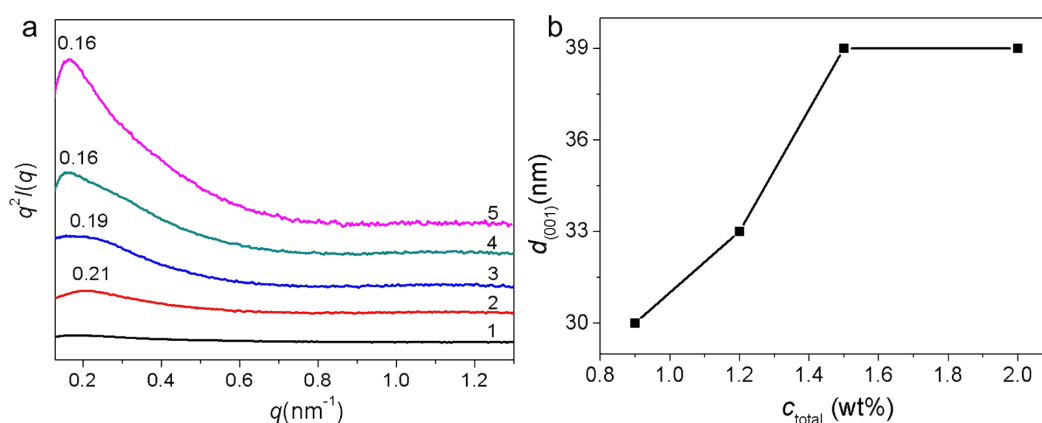


Figure S13. (a) One-dimensional SAXS patterns of the samples shown in Figure S12b. (b) The interlayer spacing $d_{(001)}$ plotted against the total concentration.

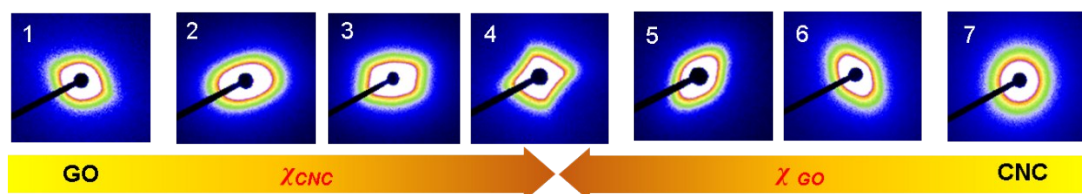


Figure S14. Two-dimensional SAXS patterns of GO, CNC and CNC/GO films with different weight fractions. The numbers 1-7 represent GO, CNC/GO (2:8 wt), CNC/GO (4:6 wt), CNC/GO (5:5 wt), CNC/GO (6:4 wt), CNC/GO (8:2 wt) and CNC, respectively.

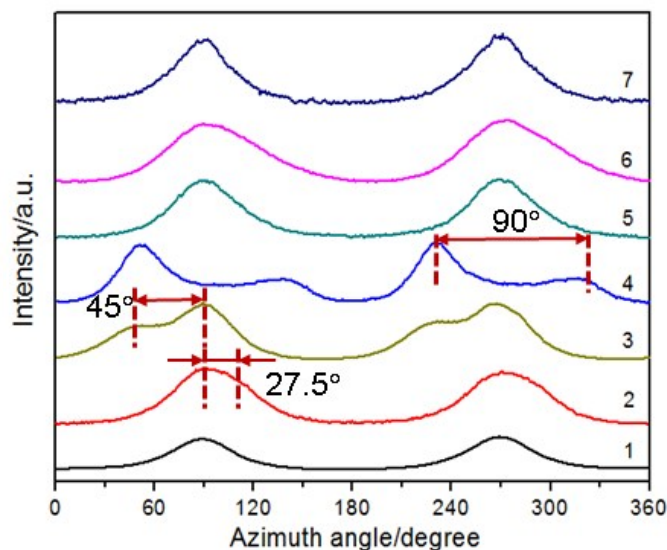


Figure S15. One-dimensional azimuthal SAXS patterns of the samples shown in Figure S14.

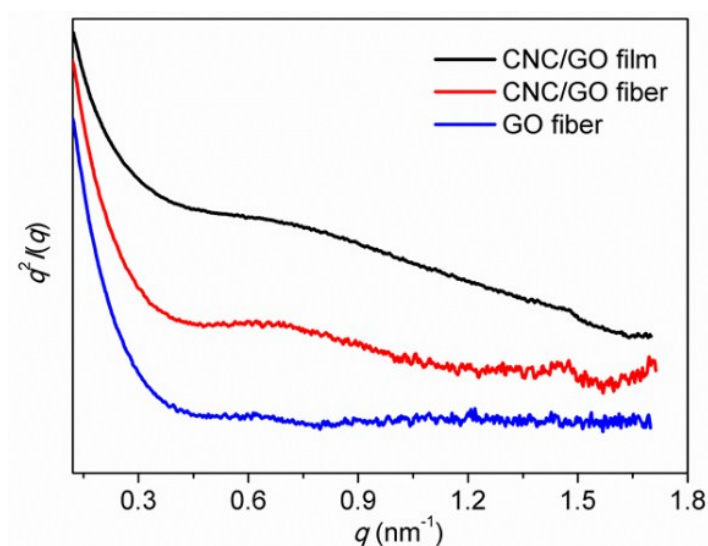


Figure S16. One-dimensional SAXS patterns of the GO, CNC/GO fiber and CNC/GO film.

References

1. X. H. Lou, H. Pan, S. M. Zhu, C. L. Zhu, Y. L. Liao, Y. Li, D. Zhang, Z. X. Chen, *Catal. Commun.*, 2015, **69**, 43-47.
2. L. Mao, S. M. Zhu, J. Ma, D. A. Shi, Y. X. Chen, Z. X. Chen, C. Yin, Y. Li, D. Zhang, *Nanotechnology*, 2014, **25**.
3. Z. H. Sun, J. J. Guo, S. M. Zhu, L. Mao, J. Ma, D. Zhang, *Nanoscale*, 2014, **6**, 2186-2193.
4. K. E. Shopsowitz, W. Y. Hamad, M. J. MacLachlan, *J. Am. Chem. Soc.*, 2012, **134**, 867-870.
5. M. K. Khan, W. Y. Hamad, M. J. MacLachlan, *Adv. Mater.*, 2014, **26**, 2323-2328.
6. S. Beck-Candanedo, M. Roman, D. G. Gray, *Biomacromolecules*, 2005, **6**, 1048-1054.
7. A. Akbari, P. Sheath, S. T. Martin, D. B. Shinde, M. Shaibani, P. C. Banerjee, R. Tkacz, D. Bhattacharyya, M. Majumder, *Nat. Commun.*, 2016, **7**.
8. S. Chen, W. Ma, Y. Cheng, Z. Weng, B. Sun, L. Wang, W. Chen, F. Li, M. Zhu, H.-M. Cheng, *Nano Energy*, 2015, **15**, 642-653.
9. H. Pan, Y. Zhang, H. Shao, X. Hu, X. Li, F. Tian, J. Wang, *J. Mater. Chem. B*, 2014, **2**, 1408-1414.
10. H. Schnablegger, Y. Singh, *The SAXS Guide (2nd)*, Anton Paar GmbH, Austria, 2011.

11. Y. Nishiyama, P. Langan, H. Chanzy, *J. Am. Chem. Soc.*, 2002, **124**, 9074-9082.
12. P. Langan, N. Sukumar, Y. Nishiyama, H. Chanzy, *Cellulose*, 2005, **12**, 551-562.
13. W. Wang, P. Zhang, S. Zhang, F. Li, J. Yu, J. Lin, *Carbohydr. Polym.*, 2013, **98**, 1031-1038.
14. E. Jin, J. Guo, F. Yang, Y. Zhu, J. Song, Y. Jin, O. J. Rojas, *Carbohydr. Polym.*, 2016, **143**, 327-335.
15. X. Ju, M. Bowden, E. E. Brown, X. Zhang, *Carbohydr. Polym.*, 2015, **123**, 476-481.
16. P. Ahvenainen, I. Kontro, K. Svedström, *Cellulose*, 2016, **23**, 1073-1086.
17. Z. Liu, Y. Ni, P. Fatehi, A. Saeed, *Biomass Bioenergy*, 2011, **35**, 1789-1796.
18. M. Zaman, H. Xiao, F. Chibante, Y. Ni, *Carbohydr. Polym.*, 2012, **89**, 163-170.
19. K. K. Sadasivuni, A. Kafy, L. Zhai, H. U. Ko, S. Mun, J. Kim, *Small*, 2015, **11**, 994-1002.
20. W. Shao, X. Liu, H. Min, G. Dong, Q. Feng, S. Zuo, *ACS Appl. Mater. Interfaces*, 2015, **7**, 6966-6973.
21. R. Xiong, K. Hu, A. M. Grant, R. Ma, W. Xu, C. Lu, X. Zhang, V. V. Tsukruk, *Adv. Mater.*, 2016, **28**, 1501-1509.
22. J. Chen, X. Zheng, H. Wang, W. Zheng, *Thin Solid Films*, 2011, **520**, 179-185.
23. D. Dinh, K. Hui, K. Hui, Y. Cho, W. Zhou, X. Hong, H.-H. Chun, *Appl. Surf. Sci.*, 2014, **298**, 62-67.
24. L. Mao, S. Zhu, J. Ma, D. Shi, Y. Chen, Z. Chen, C. Yin, Y. Li, D. Zhang, *Nanotechnology*, 2014, **25**, 215401.
25. X. M. Dong, T. Kimura, J.-F. Revol, D. G. Gray, *Langmuir*, 1996, **12**, 2076-2082.